Co-Optimization of Optical Ground Station and Network Architecture for Secure and High-Capacity Satcom Ground Segments

Romain Laigo
Cailabs
Rennes, France
romain.laigo@cailabs.com

Asher Novick
Cailabs US
Arlington, Virginia, USA

Laurie Paillier
Cailabs
Rennes, France

Cédric Dautancourt
Cailabs
Rennes, France

Julien Samaan
Cailabs
Rennes, France

Pu Jian
Cailabs
Rennes, France

Olivier Pinel
Cailabs
Rennes, France

***Abstract*—Free-space optical communication (FSOC) enables high-capacity satellite-to-ground (S2G) links but introduces strong sensitivity to atmospheric conditions, making ground segment design a key system-level challenge. This paper proposes a framework for the co-optimization of optical ground station (OGS) deployment and network architecture, jointly accounting for orbital geometry, atmospheric variability, and ground network topology. The approach combines large-scale atmospheric datasets, orbital simulations, and computationally efficient proxy metrics to enable scalable exploration of candidate OGS networks. The methodology emphasizes geographic diversity and weather decorrelation as primary drivers of network availability and performance. It further integrates practical design considerations, including link budget constraints and turbulence mitigation effects. Simulation-based case studies for a representative Earth observation constellation show that optimized OGS networks significantly outperform radio frequency (RF) architectures in terms of downlink capacity, data delivery latency, and scalability under increasing traffic demand. These results demonstrate the importance of joint infrastructure and network design for next-generation optical ground segments.**

Keywords—Laser Communication, Optical Ground Station, Ground Segment Optimization, Atmospheric Conditions, Optical Link Availability, High-Capacity Downlink

I. Introduction

The rapid growth of satellite constellations is leading to an unprecedented increase in the data volume transmitted between space and ground segments. Earth Observation (EO) missions continuously generate massive volumes of imagery that must be delivered with minimal latency, while satcom satellite constellations require high-capacity feeder links to support aggregated users' connectivity.

While radiofrequency (RF) systems remain the backbone of satellite communications, their limited throughput motivates the use of complementary technologies. Free-space optical communication (FSOC) has recently gained significant attention for satellite communications because it can provide substantially higher data rates and reduced spectrum constraints. However, optical links are more sensitive to atmospheric conditions such as cloud coverage, aerosol attenuation, and atmospheric turbulence. As a result, optical systems rely on networks of geographically distributed optical ground stations (OGS) to ensure service continuity through site diversity, with inter-satellite links (OISL) further enhancing routing flexibility when available.

The design of such networks is therefore a complex system-level problem that requires balancing orbital coverage, weather-driven link availability, and the geographical distribution of candidate sites. Previous studies have addressed this problem from different perspectives. Analytical approaches have been proposed to estimate the availability of OGS networks from cloud fraction statistics, capturing the effect of spatial correlation between sites. Reference [1] proposed approximation methods to evaluate the availability of optical ground networks based on cloud fraction datasets and probabilistic modeling of correlated atmospheric conditions. Reference [2] developed a methodology for optimizing OGS network locations using cloud-mask data and inter-site weather correlation, primarily in the context of GEO feeder links. Simulation-based approaches have also been developed to capture system-level performance: the ONUBLA study [3] analyzed access availability and throughput for Low Earth Orbit (LEO) and Geostationary Earth Orbit (GEO) optical links using cloud statistics and orbit simulations, while more recent work by Birch et al. [4] [5] evaluated data volume and latency for a commercial OGS service using long-term cloud observations. These previous studies provide important foundations for the design and analysis of optical ground networks, including methods to estimate atmospheric availability, evaluate network diversity, and simulate satellite contact opportunities.

Building upon these approaches, the present work proposes a framework for the design and system-level evaluation of OGS networks that jointly consider orbital geometry, atmospheric variability, and ground network architecture. The proposed methodology separates the optimization stage from detailed performance evaluation, enabling scalable exploration of candidate architectures while preserving accuracy in system-level assessment. It is designed to remain applicable to a wide range of optical ground segment architectures, including GEO feeder links, large LEO constellations, and ground-station-as-a-service (GSaaS)

infrastructures. In this paper, the methodology is illustrated through a case study focusing on near-real-time data delivery for a large LEO EO constellation.

II. System-Level Design Problem

The design of an OGS network can be formulated as the problem of selecting a set of ground stations that maximizes the communication performance of a given satellite system. Depending on the mission type, this performance may be expressed through different metrics defined in section V, such as link availability, total downlink capacity, or data delivery latency.

A key specificity of optical ground networks is their strong dependence on atmospheric conditions. Because optical links cannot operate through clouds, network performance depends not only on the individual availability of each station but also on the correlation of weather conditions between sites. Selecting stations solely based on their individual clear-sky availability does not necessarily lead to the best-performing network. Instead, networks benefit from geographically distributed stations experiencing uncorrelated atmospheric conditions, which increases the probability that at least one station is available at any given time.

At the same time, the orbital geometry of the satellite constellation strongly influences network performance. The geographical distribution of ground stations determines which orbital passes can be exploited for downlink opportunities. For satellite communication constellations, stations must be distributed to maintain permanent connectivity with the network, reducing outages while avoiding frequent handovers. For EO missions, the objective is often to distribute downlink opportunities across successive orbital passes in order to minimize the delay between data acquisition and delivery.

These considerations require adapting traditional ground segment design frameworks. In RF systems, site selection often prioritizes high-latitude or polar locations to maximize pass frequency, particularly for Sun-synchronous orbits. However, such strategies do not directly translate to optical systems, where atmospheric constraints can dominate link availability. As a result, OGS network design must jointly account for orbital geometry and weather conditions, leading to more geographically distributed architectures optimized for both coverage and availability.

The design of an OGS network is therefore driven by several key factors:

- the atmospheric availability of candidate sites
- the orbital geometry of the satellite constellation
- the operational objectives of the ground network
- practical constraints related to the integration of OGS within existing infrastructures

In the present work, the infrastructure constraints are addressed through a pre-selection of candidate station locations. The following sections focus on modeling the physical drivers of network performance and evaluating candidate network architecture based on orbital and atmospheric conditions.

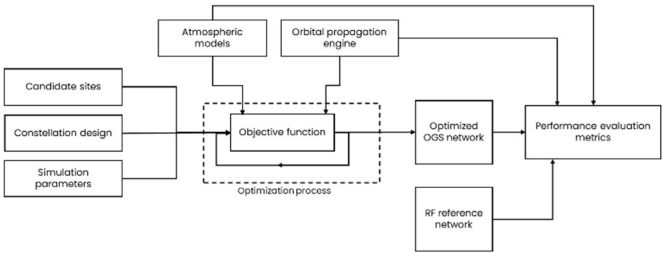

Fig. 1. Overall framework employed

Designing such networks therefore requires jointly considering satellite constellation geometry, long-term atmospheric conditions, and the geographical distribution of candidate sites. As the number of potential station locations increases, identifying the best configuration rapidly becomes a complex combinatorial problem, motivating the development of dedicated tools for the optimization and evaluation of OGS networks.

III. Modeling of Network Performance Drivers

To evaluate candidate OGS network configurations, several physical aspects influencing optical communication performance must be modeled. These include the orbital dynamics of the satellite constellation, the atmospheric conditions affecting optical link availability, and the geometric visibility between satellites and ground stations.

A. Satellite constellation modeling

Satellite constellations are represented using Walker patterns [6] [7], which provide a convenient parameterization through the number of satellites, orbital planes, altitude, and inclination. This representation allows flexible modeling of both large constellations and individual satellites while capturing the spatial distribution of satellite ground tracks. Satellite trajectories are propagated using a Keplerian orbital model. This choice allows for rapid propagation over the entire constellation via efficient vectorization, assuming strictly circular orbits and the absence of disruptions such as J2 perturbation, atmospheric friction, Sun/Moon attraction, orbital maneuvers, which is sufficient for system-level analysis over the time horizons considered in this study.

B. Atmospheric conditions modeling

Atmospheric conditions play a central role in determining the availability of OGS. Two main effects are considered in this work: cloud coverage, which can completely block optical communication, and aerosol attenuation, which introduces additional losses in the optical link budget.

1) Cloud coverage

Cloud presence is the dominant factor affecting the availability of OGS. In this study, cloud conditions are modeled using the Total Cloud Cover variable from the ECMWF ERA5 reanalysis dataset [8], which provides global atmospheric observations with a spatial resolution of 0.25° and hourly temporal resolution.

Optical communication through dense clouds is generally not feasible for space-to-ground links. For this reason, cloud impact is modeled using binary availability condition: a link is considered unavailable when the cloud coverage exceeds a predefined threshold.

2) Aerosol Attenuation

Even in clear-sky conditions, atmospheric aerosols introduce additional attenuation due to scattering and absorption of the optical signal. Atmospheric aerosols are small solid or liquid particles suspended in the air, such as dust, pollution, sea salt, or smoke. This effect is wavelength-dependent and must therefore be accounted for when estimating the performance and availability of optical communication links.

In this work, aerosol attenuation is modeled following the methodology recommended in the CCSDS Green Book *Atmospheric Data for Optical Communication Systems* (CCSDS 140.1-G-2) [9], which provides reference procedures for estimating atmospheric losses affecting optical space communication links.

The impact of aerosols on optical propagation is commonly quantified using the Aerosol Optical Depth (AOD), a dimensionless quantity representing the integrated extinction caused by aerosols along a vertical atmospheric column. According to CCSDS recommendations for optical communications, aerosol-induced attenuation can be derived from AOD using the Beer–Lambert law. For a vertical (zenith) path, the attenuation expressed in decibels is given by:

$$\tau(\lambda) = \tau(\lambda_0)\left(\frac{\lambda}{\lambda_0}\right)^{-\alpha}$$

where α is the Ångström exponent derived from AERONET spectral channels. Using this relation, AOD values at λ_0 are extrapolated to $\lambda = 1550$ nm and then converted into zenith attenuation in decibels.

A fundamental limitation of AERONET data is their local nature. Each station provides accurate information at a single geographic point, but does not describe how aerosol conditions vary spatially. To obtain a spatially continuous view, the station-based attenuation values are spatially interpolated over the globe. For any given location, the attenuation is estimated from nearby AERONET stations using a distance-weighted interpolation based on great-circle distances. Only a limited number of nearest stations are considered, ensuring that local conditions dominate the estimate and that exceptional sites do not unrealistically influence distant regions. This interpolation step does not attempt to model aerosol transport or dynamic, but it provides a pragmatic way to extend high-quality point measurements into a global field while preserving their local character. Regions with dense station coverage are strongly constrained by observations, whereas areas with sparse coverage naturally exhibit smoother, less constrained estimates.

Fig. 2 highlights the regions where aerosol attenuation is most significant. Higher losses are observed in desert regions affected by dust as well as in highly polluted areas, such as the Arabian Peninsula and Western India. The temporal distributions (Fig. 3) obtained for several representative locations are consistent with those reported in CCSDS 140.1-G-2, supporting the validity of the adopted methodology.

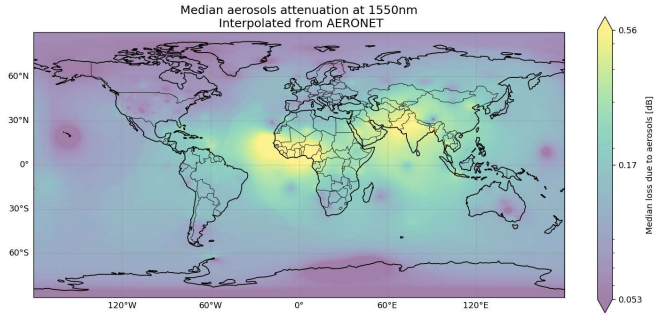

Fig. 2. Median loss at zenith obtained worldwide

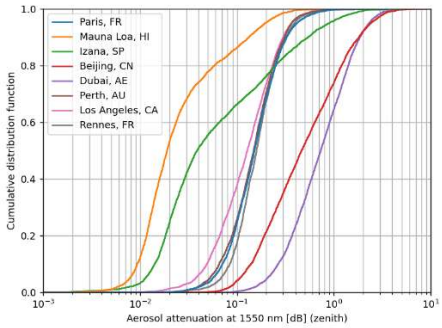

Fig. 3. Atmospheric absorption's distribution over time for a sample of locations

C. Atmospheric turbulence

In addition to atmospheric effects, the performance of OGS is also strongly influenced by design parameters, in particular the receiver aperture diameter D. While larger apertures increase the collected optical power, their effective performance is fundamentally limited by atmospheric turbulence, typically characterized by the Fried parameter r_0. The ratio D/r_0 governs the transition between photon-limited and turbulence-dominated regimes. For $D \gg r_0$, wavefront distortions across the aperture reduce coupling efficiency and lead to diminishing returns in effective link gain. Conversely, for D comparable to or smaller than r_0, the system becomes limited by photon collection and signal-to-noise ratio, with increased sensitivity to temporal fluctuations. In addition to wavefront distortions (phase perturbations), atmospheric turbulence also induces amplitude fluctuations of the received optical field, known as scintillation. These intensity variations result in random fading of the received signal and can significantly impact link reliability.

The severity of scintillation is also related to the receiver aperture size, as larger apertures tend to average out intensity fluctuations (aperture averaging), thereby reducing their impact. However, various turbulence mitigation techniques can significantly alleviate turbulence-induced impairments. In particular, adaptive optics primarily compensates for phase distortions, while TILBA-ATMO's approach can more effectively mitigate both phase distortions and amplitude fluctuations, thereby improving overall link performance [12]. As a result, practical OGS designs operate within a constrained aperture range, combined with mitigation techniques that balance these competing effects. In this work, these design parameters are incorporated through representative link budget assumptions. In particular, the impact of atmospheric effects such as aerosol attenuation and cloud cover is modeled using thresholds consistent with

realistic optical system performance. These thresholds are empirically calibrated and implicitly capture key design trade-offs, including aperture size, receiver sensitivity, and turbulence mitigation so we obtain realistic availability estimates. This approach enables a consistent system-level evaluation of network performance.

IV. OGS NETWORK OPTIMIZATION METHODOLOGY

Designing an OGS network involves selecting a subset of stations among a large set of candidate locations to maximize the performance of the resulting network. Because each station location is associated with different orbital visibility and atmospheric statistics, the performance of the network strongly depends on the combination of selected sites.

If N candidate locations are considered and the network must contain K stations, the number of possible network configurations is given by the binomial coefficient:

$$N_{solutions} = \binom{N}{K} = \frac{N!}{K!\,(N-K)!}$$

This combinatorial growth quickly makes exhaustive exploration computationally intractable for realistic problem sizes.

To mitigate this issue, the search space can first be reduced using a preselection strategy. In particular, Fuchs and Moll [2] propose a method based on single-site availability and inter-site correlation metrics. Their approach combines individual site statistics with pairwise correlation coefficients to identify and discard stations that exhibit both low availability and high correlation with other candidates, as such sites contribute little to network diversity. This preprocessing step significantly reduces the number of candidate stations and, consequently, the combinatorial complexity of the problem.

In this work, this methodology is used as a preliminary filtering stage prior to optimization. By restricting the search space to the most relevant candidate sites, the subsequent optimization process can focus on the most promising regions of the solution space. Despite this reduction, the problem remains highly non-linear, discrete, and non-differentiable due to the complex interactions between orbital coverage, atmospheric conditions, and the combinatorial nature of station selection. The resulting optimization landscape typically contains multiple local optima, making gradient-based or exhaustive approaches impractical.

To address this problem, the optimized network is identified using a stochastic search process. Starting from an initial configuration, the algorithm iteratively explores alternative station combinations by locally modifying the network composition. This exploration strategy enables efficient navigation of a complex and non-convex solution space, while avoiding premature convergence toward suboptimal configurations.

A key challenge in this optimization process is that evaluating the full performance of a ground network through time-domain simulation is computationally expensive. For this reason, the optimization process relies on computationally efficient performance metrics that approximate the expected behavior of the network while avoiding full dynamic simulations. These proxy metrics are constructed from two quantities that can be computed efficiently: the orbital ground-track density of the satellite constellation and the visibility mask of each candidate station.

A. Orbital ground-track density

The satellite constellation is first propagated over a sufficiently long-time window T (typically for several weeks). During this propagation, the subsatellite point of each satellite is recorded and projected onto the Earth's surface.

The spatial distribution of satellite ground tracks is then represented as a normalized density function $D_{orbit}(\phi, \psi)$ over latitude ϕ and longitude ψ.

In practice, this density is estimated using a 2-D histogram over a discretized latitude-longitude grid:

$$D_{orbit}(\phi, \psi) = \frac{N(\phi, \psi)}{\sum_{\phi,\psi} N(\phi, \psi)}$$

where $N(\phi, \psi)$ is the number of satellite ground-track samples inside the grid cell.

This distribution can be interpreted as the probability that a satellite of the constellation is located above a given location on Earth. This quantity only depends on the orbital architecture of the constellation and can therefore be computed once and reused throughout the optimization process, considering its distribution to be stationary over the time scales relevant for network design.

B. Station visibility mask

For a ground station located at (ϕ_g, ψ_g), satellite visibility is determined by the orbital altitude h and the minimum elevation angle θ_{min} required to establish an optical communication. These parameters define a maximum geocentric angular distance $\Delta\sigma_{max}(h, \theta_{min})$ between the station and the subsatellite point for which a line-of-sight remains feasible.

The corresponding station visibility mask is there defined over the Earth surface as :

$$LOS_g(\phi, \psi) = \begin{cases} 1, & if\ \Delta\sigma\left((\phi_g, \psi_g), (\phi, \psi)\right) \leq \Delta\sigma_{max}(h, \theta_{min}) \\ 0, & otherwise \end{cases}$$

where $\Delta\sigma$ denotes the geocentric angular distance between the candidate subsatellite point (ϕ, ψ) and the station location (ϕ_g, ψ_g).

This mask represents the region of the Earth surface from which a satellite would be visible from the station under the adopted elevation constraint. For constellations equipped with OISL, the mask can be extended to account for intra-plane and inter-plane relaying opportunities, resulting in an enhanced visibility mask used during the optimization process.

C. Scoring quantities definitions

Using the orbital density and station visibility masks introduced above, simplified performance scores are defined to guide the optimization process without relying on full time-domain simulations. These scores approximate how effectively a given network configuration provides access to

the satellite constellation, while accounting for both geometric visibility and atmospheric availability.

Two distinct optimization objectives are considered depending on the target application:

1. **Network Availability optimization** for continuous connectivity: maximizes the probability that at least one ground station can access the constellation at any given time. This naturally favors geographically distributed stations with complementary visibility and weakly correlated weather conditions.
2. **Orbital planes coverage optimization** for EO applications: maximizes access to a wide range of orbital planes, increasing the likelihood of rapidly downlinking newly acquired data. This promotes station configurations that sample different segments of the constellation ground tracks.

In both cases, the scoring functions rely on combining orbital density with station visibility and availability, providing computationally efficient proxies of system-level performance suitable for large-scale optimization.

V. Performance evaluation metrics

Once an optimized ground network configuration has been obtained, its performance is evaluated using a set of application-driven metrics. These metrics are designed to capture the key operational characteristics of the system. The following subsections introduce some of the performance metrics typically used.

A. Link availability

The instantaneous satellite-to-ground (S2G) link availability timeline is obtained from the propagation and visibility simulations described in the previous section.

At each simulation timestep t, the routing policy determines which OGS can establish an optical link with a satellite while satisfying both geometric visibility and atmospheric constraints, and assigns each station to at most one satellite. For each ground station g, a binary indicator $A_{t,g} \in \{0,1\}$ denotes whether a S2G link is active. The average link availability for each station can be computed as:

$$A_g = \frac{1}{T}\sum_t A_{t,g}$$

And the global network availability as:

$$A = \frac{1}{T}\sum_t \left(1 - \prod_g \left(1 - A_{t,g}\right)\right)$$

B. Downlink capacity

Each active link provides a nominal downlink throughput R_g. The total downlink capacity available to the constellation at time t is therefore the sum of the capacities of all active ground stations:

$$C_t = \sum_g A_{t,g}\, R_g$$

C. Capture to delivery latency

This metric represents the time elapsed between the acquisition of a scene onboard a satellite and the moment when the corresponding data volume has been fully transmitted to the ground network. To evaluate this quantity, we use the simulated timeline of satellite-to-ground transmission opportunities.

The actual transmitted volume depends both on the availability of a satellite–ground link and on the amount of data stored onboard the satellite. In practice, a satellite will only transmit data when it is connected to an OGS and when data are available in its onboard buffer. We therefore denote by $S_{t,s}$ the volume of data effectively transmitted by satellite s during timestep t. The cumulative transmitted volume is therefore:

$$V_{t,s} = \sum_{\tau=0}^{t} S_{\tau,s}$$

For an EO image of size V_{img} captured at time t_0, the delivery time t_{del} is defined as the earliest time at which the cumulative transmitted volume exceeds the required data volume:

$$t_{del} = \min_{t \geq t_0} \{V_{t,s} - V_{t_0,s} \geq V_{img}\}$$

The capture-to-delivery latency is then

$$L_{c2d} = t_{del} - \mathrm{t}_0$$

This formulation naturally accounts for the discrete nature of satellite passes and the time-varying downlink capacity resulting from orbital dynamics and atmospheric availability. If the data volume cannot be entirely transmitted during a single pass, the remaining data are progressively downlinked during subsequent contacts until the full product has been delivered.

D. Congestion and concurrent tasking

In addition to isolated image delivery latency, we evaluate network congestion under concurrent tasking, which is critical for EO missions where multiple acquisitions may be generated before previously acquired data have been fully downlinked. In such situations, the limiting factor is not only the existence of ground contacts, but also the amount of data that can be evacuated during each contact.

To capture this effect, each satellite is modeled as maintaining an onboard first-in first-out (FIFO) queue that stores acquired data awaiting transmission. At each simulation step, newly acquired data are added to the onboard buffer, while data are removed according to the available downlink capacity during satellite-to-ground contact opportunities. As a result, the buffer level evolves over time depending on the balance between incoming data and transmission capability.

To emulate concurrent tasking activity, acquisition requests are generated stochastically using a Poisson process whose rate corresponds to a prescribed daily tasking volume. Each request produces a data product of fixed size V_{img}, which is inserted into the satellite's transmission queue and

progressively downlinked during successive contact opportunities depending on the available capacity.

The capture-to-delivery latency of a given product k is defined as the time elapsed between its acquisition time t_k^{cap} and the time at which its full data volume has been transmitted to the ground network:

$$L_{c2d_k} = t_k^{del} - t_k^{cap}$$

where t_k^{del} is the first time for which the cumulative transmitted volume exceeds the cumulative data volume of all preceding queued products including product k, considering that each product contributes a volume V_{img} to the queue.

VI. Case Study: Optical Ground Network for Near Real-Time High-Volume Data Delivery

A. Mission scenario

To illustrate the proposed framework, we consider a representative EO mission scenario and evaluate the performance of different OGS network architectures for high-volume data delivery.

The simulated space segment consists of a constellation of 48 LEO satellites in a sun-synchronous orbit at 550 km altitude, distributed over 6 orbital planes with an inclination of 97.7°. Such architecture enables frequent revisit of most locations on Earth, with maximum revisit intervals on the order of a few hours. Each satellite is equipped with a laser communication terminal capable of transmitting data to OGS at a signaling rate of 10 Gbps, corresponding to an effective throughput of approximately 7.35 Gbps after protocol overheads. During nominal operations, each satellite acquires Synthetic Aperture Radar (SAR) imagery over land areas except poles, and stores the generated data onboard until a downlink opportunity becomes available.

TABLE I. Parameters Used for the Simulation

Simulation parameter		Value	
Satellites constellation	Number of satellites	48	
	Number of orbital planes	6	
	Altitude	550 km	
	Planes inclination	97.7°	
	Constellation design	Walker Delta	
	Phasing parameter	0	
Ground stations	Type	OGS	X-band antenna
	Downlink net useful throughput	7.35 Gbps	300 Mbps
	Minimum elevation angle	20°	10°
	Weather impact	Clouds & aerosols	None

For the latency analysis, we consider representative EO products that are several tens of gigabytes in size, corresponding to high-resolution SAR scenes. A typical image size of 35 GB is used to evaluate capture-to-delivery latencies. For comparison, a reference RF architecture based on 10 X-band gateways operating at 300 Mbps is also evaluated using a deployment representative of existing RF network practice (see Fig. 5).

The optical ground networks considered in this study are derived from the optimization framework described in Section IV, which takes as input a set of 137 candidate sites (Fig. 4) among existing teleports and subsea cable landing stations, selected for their access to existing ground infrastructure, making them suitable candidates for realistic OGS deployment. The framework is first used to identify an optimal 25-OGS network. It is then further exploited to extract prioritized subsets of 10, 5, and 2 OGS, allowing the performance of intermediate-size networks to be assessed using consistent selection criteria.

Fig. 4. 137 candidate sites provided to the optimization process

B. Simulation results

The optimized network shown in Fig. 5 is obtained using the orbital planes coverage metric introduced in Section IV.C to maximize access to a wide range of orbital planes, which directly supports low-latency data delivery for EO missions. This leads to a geographically spread network, with OGS positioned to capture complementary segments of the constellation's ground tracks. Due to their poor cloud-free availability, polar sites are not selected in the first stages of the optimization and are not well suited for small networks. However, their relevance increases as the number of OGS grows, where they contribute to densifying pass opportunities and further improving global coverage.

Fig. 5. 25 OGS ground network resulting from the optimization process (left) and comparative ground network for the RF X-band segment (right)

Concerning aggregated downlink capacity, Fig. 6 shows the average daily volume of data successfully downloaded from the constellation for different OGS network sizes. With a 10-OGS network, the average daily downloaded volume reaches approximately 100 TB, with a standard deviation of 23 TB, reflecting the impact of weather variability over the simulated period. Even an initial 2-OGS network already provides about 24.4 TB per day on average, showing that a small but geographically diverse optical network can already exploit a significant fraction of the available passes. Increasing the number of stations progressively improves network throughput by both increasing the number of accessible passes and mitigating weather-induced link interruptions. Comparatively, despite the absence of weather-related interruptions, the lower RF data rate significantly limits the

achievable throughput. The RF network provides a constant daily downlink capacity of about 20 TB.

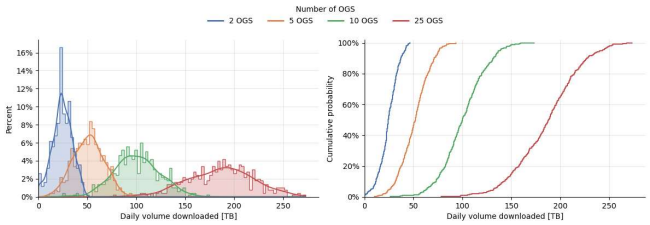

Fig. 6. Daily downlink capacity obtained for several OGS networks

Beyond throughput, the simulations also evaluate the capture-to-delivery latency, defined as the time between the acquisition of an EO image and the completion of its download to the ground network. The results (Fig. 7) show that increasing the number of OGS significantly shifts the latency distribution toward shorter delays. For example, with 10 OGS, the average delivery latency for a 35 GB SAR scene is 1hour 50min, while larger networks with 25 stations reduce this average to 1hour 07min.

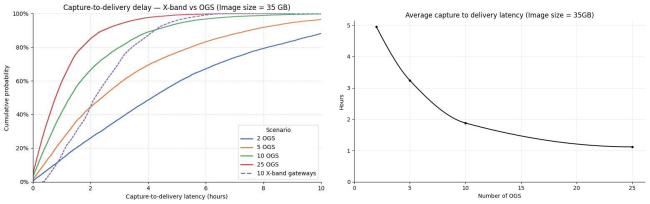

Fig. 7. Distribution of capture to delivery delays through several ground architectures (left) and evolution of average delivery delays with the number of OGS in the network (right).

The difference with RF ground architecture is explained by the amount of data that can be transferred during a single satellite pass: with 10 Gbps optical downlink, a 35 GB SAR scene can typically be fully transmitted during a single pass, and several scenes can even be delivered within the same contact. In contrast, the much lower throughput of the 300 Mbps X-band link prevents a full scene from being downloaded in a single pass. As a result, multiple successive passes are often required to complete the transmission of a large EO product, which directly increases delivery latency.

Single-capture latency, however, remains optimistic for operational EO systems, because in practice multiple acquisitions compete for the same downlink resources. Service Level Agreement (SLA) under concurrent tasking is assessed by progressively increasing the daily ordered volume and measuring the fraction of products delivered within fixed latency targets. Fig. 8 highlights a strong divergence in scalability between RF and optical ground segments. Optical architectures exhibit a limited degradation with load, while RF rapidly saturates. For the 3-hour SLA (right), a 10-OGS network maintains ~75% SLA up to 40TB/day, and still delivers 40% at 100TB/day. The 25-OGS configuration is highly resilient, sustaining 90% compliance up to 50TB/day and remaining above 80% for higher load.

In contrast, the X-band architecture shows a sharp collapse: compliance drops below 20% as early as ~20 TB/day and falls to only a few percent beyond 40 TB/day. This behavior reflects the hard capacity limit of the RF downlink, beyond which the system quickly enters a congestion regime with growing queues and missed latency targets.

The same pattern is observed for the 1-hour SLA (left), with overall lower compliance levels but identical scaling trends. Optical networks degrade smoothly with increasing demand, whereas RF performance collapses once the ordered volume approaches its aggregate daily downlink capacity. These results show that optical ground segments not only increase capacity, but also fundamentally change how the system behaves under load, enabling it to handle increasing demand more efficiently.

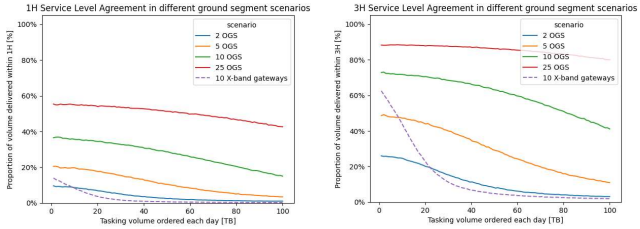

Fig. 8. Service Level Agreement compliance versus daily tasking volume for different ground segment architectures: 1-hour SLA (left) and 3-hour SLA (right).

VII. Conclusion

Driven by the rapid growth of EO data and large satellite constellations, traditional RF ground segments are reaching fundamental capacity limits. In this context, this paper introduced a co-optimization framework that jointly addresses OGS deployment and network architecture design by combining orbital geometry, atmospheric conditions, system-level performance metrics, and implicit terminal design assumptions such as receiver aperture sizing. The results highlight the critical role of geographic diversity and weather decorrelation in maximizing availability and demonstrate that optical ground networks significantly outperform RF architectures in throughput, latency, and scalability under increasing data demand. This approach provides a practical foundation for designing next-generation high-capacity ground segments and supports the transition toward scalable, hybrid optical satellite communication infrastructures.

References

[1] M. Sanchez Net, I. Del Portillo, E. Crawley, and B. Cameron, "Approximation Methods for Estimating the Availability of Optical Ground Networks," *J. Opt. Commun. Netw.*, vol. 8, no. 10, p. 800, Oct. 2016, doi: 10.1364/JOCN.8.000800.

[2] C. Fuchs and F. Moll, "Ground Station Network Optimization for Space-to-Ground Optical Communication Links," *J. Opt. Commun. Netw.*, vol. 7, no. 12, p. 1148, Dec. 2015, doi: 10.1364/JOCN.7.001148.

[3] C. Fuchs, "Assessment of access availability of space-ground optical links," ESA, 2017.

[4] M. Birch *et al.*, "Availability, outage, and capacity of spatially correlated, Australasian free-space optical networks," *J. Opt. Commun. Netw.*, vol. 15, no. 7, p. 415, Jul. 2023, doi: 10.1364/JOCN.480805.

[5] M. Birch, H. Sundberg, and M. Sans, "Developments of an optical ground station network for LEO-to-ground satellite data services," 2025.

[6] J. G. Walker, "Satellite constellations," JBIS, vol. 37, p. 559, 1984.

[7] I. Leyva-Mayorga *et al.*, "NGSO constellation design for global connectivity," *arXiv preprint* arXiv:2203.16597, Mar. 2022

[8] H. Hersbach *et al.*, "ERA5 hourly data on single levels from 1940 to present," 2023, doi: 10.24381/cds.adbb2d47.

[9] CCSDS, "Real-Time Weather and Atmospheric Characterization Data," 2024. [Online]. Available: https://ccsds.org/Pubs/140x1g2.pdf

[10] B. N. Holben *et al.*, "AERONET—A Federated Instrument Network and Data Archive for Aerosol Characterization," *Remote Sens.*

Environ., vol. 66, no. 1, pp. 1–16, Oct. 1998, doi: 10.1016/S0034-4257(98)00031-5.

[11] D. M. Giles *et al.*, "Advancements in the AERONET Version 3 database," *Atmospheric Meas. Tech.*, vol. 12, no. 1, pp. 169–209, 2019, doi: 10.5194/amt-12-169-2019.

[12] C. Abbouab *et al.*, "Latest results and perspectives of TILBA-ATMO system for LEO satellite to ground optical links following SDA & CCSDS standards," in *Proc. IEEE Int. Conf. Space Optical Syst. Appl. (ICSOS)*, Kyoto, Japan, 2025, doi: 10.1109/ICSOS66026.2025.11443183.